JOURNAL OF SPACECRAFT AND ROCKETS
Vol. 30, No. 1, January-February 1993

Analysis of Inviscid and Viscous Hypersonic Flows past a Two-Stage Spacecraft

Wolfgang Schröder* and Gerhard Hartmann*
Deutsche Aerospace AG, 8000 Munich 80, Germany

A detailed study of inviscid and viscous hypersonic flows over a two-stage space transportation system at a gap width between upper and lower stage $\Delta z_r = 2.24$ m has been made. We numerically integrated the three-dimensional Euler and Navier-Stokes equations for perfect and/or equilibrium real-gas flows. The qualitative and quantitative comparison of experimental and numerical data at several relative angles of attack showed good agreement with regard to lift, drag, and pitching moment coefficients and proves the numerical scheme to be a useful device for the meticulous analysis of flows over parallel-staged reusable launch vehicles. It showed for inviscid and viscous flowfields that the impact of the upper stage on the flow over the lower stage decreases when the incidence angle to each other is increased and that the influence of the shock pattern within the gap between space vehicle and aircraft on the aerodynamic characteristics of the orbiter is less at higher relative angles of attack. The results of an inviscid perfect-gas and an inviscid equilibrium real-gas flow evidence the validity of the perfect-gas assumption for the problems investigated.

Nomenclature

c_d	= drag coefficient of upper stage
c_f	= skin-friction coefficient
c_l	= lift coefficient of upper stage
c_p	= pressure coefficient
c_{pm}	= pitching-moment coefficient of upper stage
l	= length of upper stage, mm (see Fig. 1)
M_∞	= freestream Mach number
p	= static pressure, N/m^2
Re_∞	= freestream Reynolds number based on upper-stage length
T_∞	= static freestream temperature, K
T_0	= stagnation temperature, K
$x/l, y/l, z/l$	= nondimensional coordinates (see Fig. 1)
α	= angle of attack of lower stage, deg
β	= yaw angle, deg
Δz_r	= gap width of real configuration, m
$\Delta\alpha$	= relative angle of attack between upper and lower stage, deg

Introduction

IN the past several years, the investigation of single- and two-stage winged space transportation systems has seen a resurgence because of, among other factors, the theoretically more favorable launch cost/payload ratio.The spectrum of the conceptual design studies ranges from the single-stage National Aero-Space Plane (NASP) in the United States to the two-stage space transportation system (SAENGER) in Germany. Both vehicles are high lift over drag transport configurations that take off horizontally from a runway. NASP flies into a low Earth orbit and then returns to an airport, whereas in the case of the two-stage spacecraft, a separation maneuver is carried out at an altitude of approximately 35 km. In principle, the stage separation is proposed as follows. With a strut mechanism, the upper stage is lifted to a certain incidence angle and a minimum gap width between the stages. In addition, the thrust of the orbiter is used to generate sufficient lift for the separation maneuver. Thereafter, the lower stage returns to the launch site for horizontal landing and the completely reusable upper stage flies into an orbit.

During the staging maneuver, the stages are in close proximity, and aerodynamic interactions between the vehicles may cause significant effects on the aerodynamic characteristics of each vehicle. The separation maneuver is finished when the distance between the stages is large enough such that no more interferences between them occur.The present study deals with the analysis of the interactions when the gap width is so small that the flow of the upper stage immediately affects the flight conditions of the lower stage and vice versa.

Unlike the standard separation of vehicles of different size in which only the flight conditions of the smaller stage are noticeably perturbed, the separation of two vehicles of comparable size can mutually impair the aerodynamics of both stages. For this reason, the analysis of the flowfields at staging is extremely important. To our knowledge, little work has so far been published on the investigation of such separation maneuvers at supersonic and/or hypersonic speeds. In Ref. 1 an experimental analysis of the stage separation of parallel-configured launch vehicles was conducted at Mach numbers 3 and 6 and, with these experimental data, results of the complete separation maneuver based on the integration of the kinematical equations of motion were obtained. A similar approach was applied in Ref. 2, in which slender body theory provided the input data to solve the equations of motion. The most recent experiments[3] were focused on the investigation of the flow at small gap widths between the stages, i.e., at a state with aerodynamic interactions between both vehicles. The results in all of these studies indicate that the separation of parallel-arranged launch vehicles is very sensitive to any perturbation in the flowfield, and that a detailed analysis of the configuration is necessary to determine the conditions for a safe separation maneuver.

We do not know of any numerical study of the flowfield at such separation maneuvers. Our first attempt to investigate the flow when both stages are in close proximity was based on solutions of the two-dimensional Navier-Stokes equations. However, the comparison with experimental data[3] demonstrated a drastically varying discrepancy for the aerodynamic coefficients. Besides, some of the flowfields computed were unsteady due to an unsteady separation bubble, whereas the measurements definitely showed a steady flow. The separation occurred on the upper surface of the lower stage right under the nose of the upper stage. The separation bubble caused a

Received May 11, 1992; revision received July 20, 1992; accepted for publication July 20, 1992.

*Research Scientist, Space Communications and Propulsion Systems Division, Fluid Dynamics, P.O. Box 801169.

compression wave that strengthened the bow shock of the upper stage, which again increased the separation. The reverse flow regime grew until the flowfield between the nose of the upper stage and the aircraft was completely subsonic such that the bow shock vanished in this region. Thereafter, the separation bubble was reduced down to its initial size. The bow shock was regenerated, which, together with the compression wave of the separation bubble, resulted again in an extension of the reverse-flow regime. Such an oscillation has never been observed in the experiments. That is, the assumption of a two-dimensional flow resulted in unphysical solutions and, therefore, the three-dimensional conservation equations are solved in this paper. A relaxation method whose results have been proven for several three-dimensional problems[4,5] was used to compute the flow.

The purpose of this paper is the numerical analysis of the flow over vehicles that are arranged in close proximity for launch. The experiments[3] are a guideline inasmuch as, without taking into account the strut mechanism, only the static aerodynamics are analyzed, i.e., the relative position of both stages to each other is kept fixed. The computation of the complete dynamic separation maneuver is beyond the scope of this study. The method is demonstrated to simulate the flowfield between parallel-configured vehicles with satisfactory accuracy based on an experimental-numerical comparison. For this reason, the scheme is deemed the proper basis for further developments so that, finally, flows over two-stage systems can be numerically tackled that currently cannot be experimentally simulated. The flow conditions that occur at release of the two stages (the second stage is already at an initial spacing distance and attitude with respect to the first stage) are investigated. The gap width chosen is $\Delta z_r = 2.24$ m, since experimental data are available for this configuration. Several incidence angles between the stages are computed. The quality of the numerical results is shown by a qualitative and quantitative comparison with measurements[3] using schlieren photographs, density contours, and aerodynamic coefficients.

Numerical Approach

The three-dimensional Euler and/or Navier-Stokes equations for a perfect and/or an equilibrium real gas are solved by a second-order finite-volume Newton-type relaxation method.[4-6] The viscous terms are approximated by central differences and the discretization of the Euler terms is based on a symmetric total variational diminishing scheme[7,8] using a Roe-averaged[9,10] four-argument minmod limiter. For further details concerning the numerical method and the boundary conditions, see Refs. 4–6, and 11.

A two-block mesh is used.[11] The outer O-H grid consists of $51 \times 146 \times 95$ normal $\times$ streamwise $\times$ spanwise cells and covers the region between the outermost boundary, the interface of the two blocks, and the lower and upper surfaces of the lower and upper stages. The gap between the upper and lower stage is resolved by an inner $40 \times 146 \times 35$ cell grid, resulting in a 911,770-cell mesh. This structure extends over the total length of the lower stages. The minimum normal step size is $\Delta n/l = 10^{-4}$. To get an idea of the grid dependence of the aerodynamic coefficients, we conducted some calculations on a coarser 179,250-cell mesh in which the outer block contains $26 \times 75 \times 65$ cells and the inner block $20 \times 75 \times 35$ cells.

Results

In the following, the flow over a two-stage space transportation system (STS) is analyzed. The scale factor of the wind-tunnel model (Fig. 1) is 1:160. The flow parameters are the same as in the experiments.[3] At $M_\infty = 6$, $Re_\infty = 1.13 \times 10^6$, $T_\infty = 242$ K, $\alpha = 0$ deg, $\beta = 0$ deg, and a gap width at the aft end of the fuselage of the upper stage of $\Delta(z/l) = 0.083$ for the wind-tunnel model, i.e., $\Delta z_r = 2.24$ m for the real configuration, the hypersonic flowfield is investigated by integrating numerically the Euler and/or Navier-Stokes equations. The

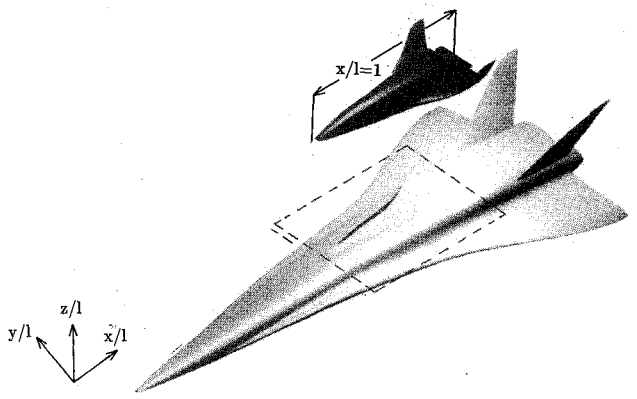

Fig. 1 Wind-tunnel model of the two-stage transportation system. The reference length is 1 = 167.7 mm. The dashed rectangle defines the region of the closeup view shown in Fig. 8.

relative angle of attack is varied within the range $\Delta\alpha = 0$, 2, and 4 deg, which causes an increase of the gap between the stages in the nose region of the upper stage. Based on the experimental results,[3] a laminar flowfield is assumed. Unless otherwise stated, perfect-gas flows are considered. In our numerical-experimental comparison we contrast the aerodynamic coefficients of the upper stage. Since we assume the impact of the winglets for these quantities to be negligible, the numerical upper-stage model has no winglets. Moreover, since the experimental values of the aerodynamic coefficients are based on a constant ($p = 0$) state in the wake of the upper stage, we do not compute the wake flow of the upper stage, i.e., the outflow boundary coincides with the trailing edge of the fuselage of the upper stage. That is, the flowfield over the rear part of the lower stage is not considered here, and as such, no aerodynamic coefficients of the lower stage are computed in this study.

The coarse grid code requires a memory of 59.7 Mbyte and the fine grid version 268.6 Mbyte. On a Fujitsu/SNI VP200, it takes approximately 15 CPU hours to determine a converged fine grid solution of the viscous flowfield, and about 7 CPU h for the inviscid flowfield. The solution is considered converged if the $\mathcal{L}_2$-norm of the residual of the energy equation has dropped at least four orders of magnitude, and if the sum of the maximum differences of the local c_p and c_f values is less than 10^{-3} within the last 50 iterations.

Throughout the discussion of our solutions, the following notation is used: the upper stage is called the space vehicle and the lower stage the aircraft. We start with a detailed presentation of the inviscid and viscous flowfield over the STS; subsequently, we contrast numerical solutions and experimental data qualitatively and quantitatively and, thereafter, the comparison of an inviscid perfect gas and equilibrium real-gas flow past the hypersonic two-stage transportation system winds up the discussion of the results.

Inviscid Flow past an STS

We turn now to the comparison of the inviscid flows at different incidence angles. Because of the hypersonic flow conditions, it goes without saying that the alterations of the flow, caused by varying $\Delta\alpha$, occur only downstream of the bow shock of the upper stage. The flow below the lower stage, the location of the bow shock wave of the lower stage, the thickness of the thin layer that covers the forebody of the aircraft, and the expansion on the upper surface of the lower stage at the edge of the trough, all of these flow phenomena remain unaltered when $\Delta\alpha$ is increased (Fig. 2). The location of the interaction of the bow shock of both stages moves from the space vehicle's leeward side at $\Delta\alpha = 0$ deg down to the nose at $\Delta\alpha = 2$ deg (Fig. 2), reaches the windward side of the upper stage at $\Delta\alpha = 4$ deg and, as such, reduces the maximum pres-

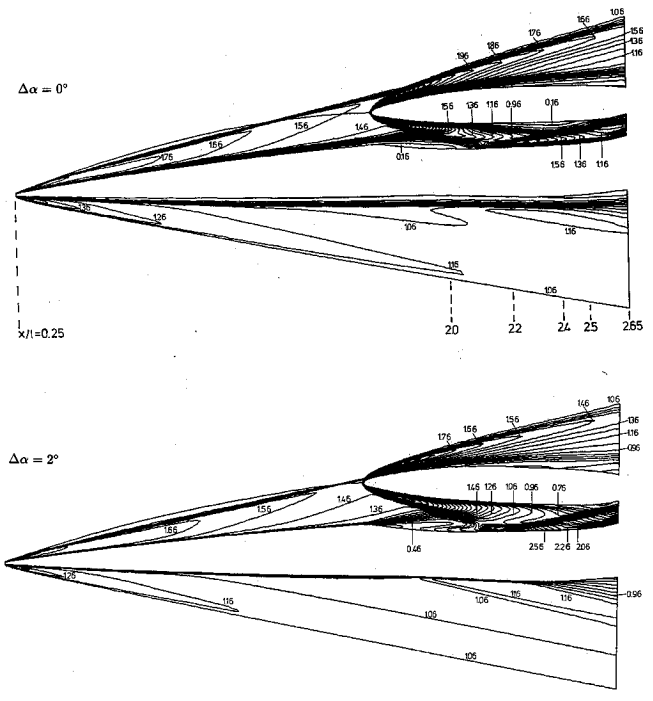

Fig. 2 Density contours in the symmetry plane at $\Delta\alpha = 0$, 2 deg. [inviscid flow, $(\rho/\rho_\infty)_{min,max,\Delta} = 0.16, 9.40, 0.1$].

sure at the nose. The location of the space vehicle's bow shock relative to its lower surface is hardly affected when $\Delta\alpha$ is increased, resulting in a larger shock angle at higher relative angles $\Delta\alpha$. Nevertheless, the shock impingement point on the upper surface of the aircraft is clearly shifted downstream because of the relatively small gap width $\Delta z_r = 2.24$ m (Fig. 2). That is, when $\Delta\alpha$ is enlarged, stronger positive pressure gradients occur further downstream on the upper surface of the lower stage. For this reason, the reflected shock wave clearly impinges on the lower surface of the space vehicle for $\Delta\alpha = 0$ deg, whereas at $\Delta\alpha = 2$ deg a shock-surface interaction can be observed just before the outflow boundary (Fig. 2), and for $\Delta\alpha = 4$ deg no shock-surface interaction takes place, although the shock angle of the reflected shock at $\Delta\alpha = 4$ deg is larger than that at $\Delta\alpha = 0$ deg.

The dependence of the shape and location of the reflected compression wave on $\Delta\alpha$ is also evidenced by the density contours in the cross section $x/l = 2.55$ (Fig. 3). At $\Delta\alpha = 0$ deg the shock wave has already impinged on the space vehicle's lower surface and the impingement trace drifts away from the symmetry plane, whereas at $\Delta\alpha = 4$ deg the entire shock wave in the spanwise direction has just been reflected from the upper surface of the fuselage of the aircraft. Thus, the interaction between the upper and lower stage decreases at higher relative angles of attack $\Delta\alpha$. The bow shape of the reflected wave is also evidenced in those illustrations. Furthermore, the independence of the leeward interaction location of the bow shocks of both stages on $\Delta\alpha$ is shown in Fig. 3.

In Fig. 4 the c_p distribution at several cross sections on the surface of the aircraft is shown. Unfortunately, at the present time no experimental c_p data are available.The computational results indicate 1) the dependence of the strength of the space vehicle's bow shock on $\Delta\alpha$, 2) the downstream shift of the shock impingement point when $\Delta\alpha$ is increased, 3) the development of the shock-surface interaction in the spanwise direction, and 4) the region in which the flow is influenced by the increase in $\Delta\alpha$. At $\Delta\alpha = 0$ deg the maximum pressure coefficient $c_{p,max}$ ($\Delta\alpha = 0$ deg) = 0.15 occurs at approximately $x/l = 2.2$, and for $\Delta\alpha = 4$ deg the location of $c_{p,max}(\Delta\alpha = 4$ deg) = 0.23 is shifted downstream to $x/l = 2.4$. The further upstream the shock impinges on the surface, the larger the spanwise extension of the pressure plateau. Using the results of the spanwise c_p distribution, one can determine the domain on the upper surface of the aircraft ($y/l \leq 0.35$) in which the flowfield is altered when $\Delta\alpha$ is enlarged. Thus, based on these findings, in future studies an artificial boundary in the spanwise direction can be defined to avoid the recomputation of the flow over the complete lower stage when $\Delta\alpha$ is varied in an inviscid flow, thus reducing the computational costs.

Viscous Flow past an STS

We turn now to discuss the viscous flow over the space-transportation system at various relative angles of attack. The cell Reynolds numbers at the surface of the fine grid solution $1 \leq Re_{cell,s} \leq 5$ seem to be adequate to resolve gradients at the wall. In Fig. 5 the density contours in the symmetry plane at $\Delta\alpha = 0$ and 2 deg are shown. Compared with the solution of the inviscid flow in Fig. 2, the development of the boundary layer is very evident. Because of that, the bow shock of the aircraft causes a slightly higher pressure rise than in the inviscid flow. This is visualized by the small increase in the shock angle in Fig. 5. Furthermore, the strong expansion at the edge of the trough no longer occurs. As far as the flow pattern within the gap is concerned, it is clear when the Euler and Navier-Stokes solutions are contrasted, that the smaller $\Delta\alpha$ the more evident are the viscous-inviscid differences since in fractions of the local gap width, the thickness of the boundary layer is enlarged if $\Delta\alpha$ is reduced. Except for the small portion of the separation region upstream of the impingement point of the bow shock of the upper stage on the surface of the aircraft (see Fig. 8), the part of the flowfield that changes at different $\Delta\alpha$ is located downstream of the bow shock of the space vehicle. As in the inviscid investigation, the location of the shock-shock interaction slides from the leeward side downward when $\Delta\alpha$ is increased. However, at $\Delta\alpha = 2$ deg this interaction takes place a bit further away from the tip of the nose of the space vehicle than in the inviscid case. At larger $\Delta\alpha$ the shock impingement point on the upper surface of the

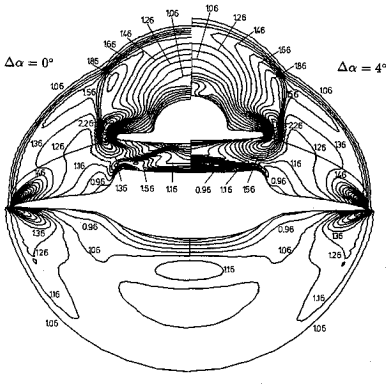

Fig. 3 Density contours $[(\rho/\rho_\infty)_{min,max,\Delta} = 0.16, 9.40, 0.1]$ of the inviscid flowfield at $x/l = 2.55$ at $\Delta\alpha = 0$ deg (left) and $\Delta\alpha = 4$ deg (right).

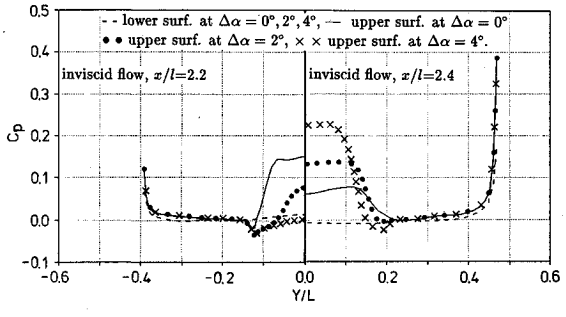

Fig. 4 Pressure coefficient c_p as a function of span of the lower stage at two cross sections.

aircraft moves downstream and, therefore, the reflected shock for $\Delta\alpha = 4$ deg does not strongly interfere with the lower side of the space vehicle (see Fig. 6).The larger the $\Delta\alpha$, the less the flow on the windward surface of the upper stage is influenced by the reflection of the bow shock on the upper surface of the lower stage. This means that, when $\Delta\alpha$ is large enough, the shock pattern within the gap has no more impact on the aerodynamic coefficients of the upper stage. This is true for inviscid and viscous flow.

In Fig. 6 the density contours illustrate the spanwise flowfield at the cross section $x/l = 2.55$. It is easy to see the bow shocks of the upper and lower stages and the independence of their interaction locus on $\Delta\alpha$. To identify the shape and locations of the shock waves within the gap, it is recommended that one compares the viscous flowfield with the inviscid solution displayed in Fig. 3. At $\Delta\alpha = 0$ deg the compression wave in the spanwise direction seems to be mostly swallowed by the viscous forces. At least no density gradient can be detected that is comparable in location and shape with that of the inviscid flowfield. For $\Delta\alpha = 2$ deg the shock is already relatively close to the lower surface of the upper stage.[11] At $\Delta\alpha = 4$ deg the reflected shock wave is located approximately midway between the stages; it has just been formed downstream of the reverse-flow region on the aircraft.

The pressure distributions on the surface of the aircraft resemble those of the inviscid flow. For this reason we do not present the c_p distributions of the Navier-Stokes solutions here, but discuss only the c_f distribution at several cross sections of the aircraft (Fig. 7). A comparison with experimentally determined c_f values cannot be conducted since skin-friction values have not been measured yet. To evidence the presentation of the wall shear stress computed and to give an overall impression of the flow in the immediate proximity of the lower-stage surface, we also show in Fig. 8 a partial view of the wall streamlines on the aircraft. For $\Delta\alpha = 0$ deg the shock-boundary-layer interaction causes a streamwise separation bubble ($c_f < 0$) at $x/l = 2.0$ that extends in the spanwise direction over the entire trough, whereas at $\Delta\alpha = 2$ deg only the flow close to the edge of the trough is reversed in this cross section and at $\Delta\alpha = 4$ deg no separation occurs (Fig. 7). This

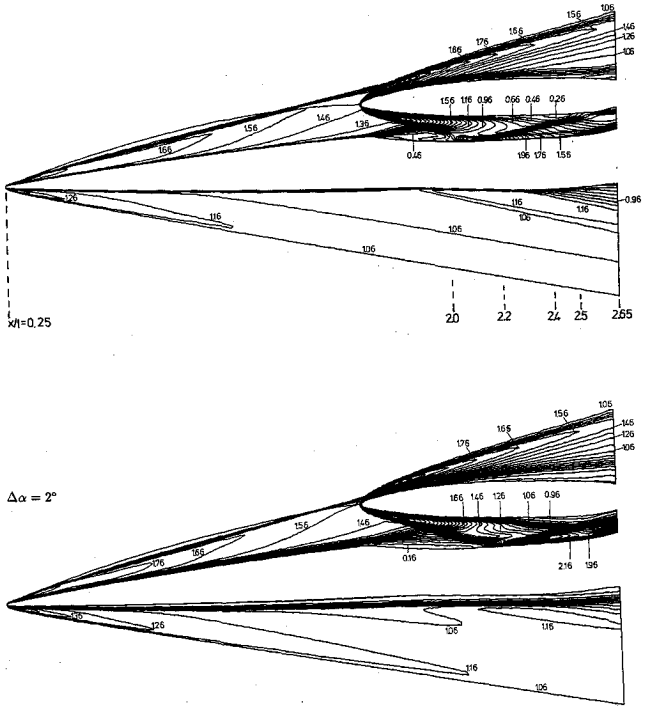

Fig. 5 Density contours in the symmetry plane at $\Delta\alpha = 0$, 2 deg [viscous flow, $(\rho/\rho_\infty)_{min,max,\Delta} = 0.16, 9.40, 0.1$].

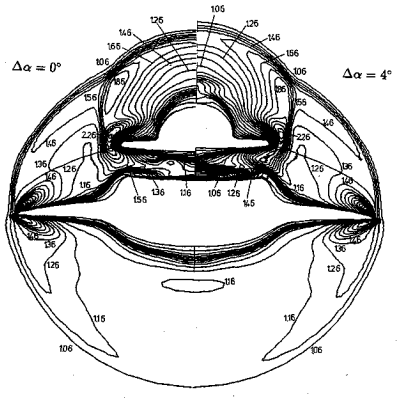

Fig. 6 Density contours $[(\rho/\rho_\infty)_{min,max,\Delta} = 0.16, 9.40, 0.1]$ of the inviscid flowfield at $x/l = 2.55$ at $\Delta\alpha = 0$ deg (left) and $\Delta\alpha = 4$ deg (right).

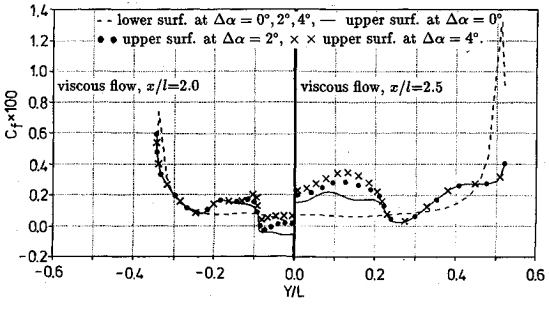

Fig. 7 Skin-friction coefficient c_f as a function of span of the lower stage at two cross sections.

flow pattern changes drastically when we consider cross sections at higher x/l values. At $x/l = 2.1$ the flow is completely reversed within the trough at $\Delta\alpha = 2$ deg, at $\Delta\alpha = 0$ deg most of the flow has already reattached, and at $\Delta\alpha = 4$ deg the separation just sets in. Further downstream a massive separation occurs at $\Delta\alpha = 4$ deg, whereas for $\Delta\alpha = 2$ deg a small reverse-flow region is located mainly near the edge of the trough and for $\Delta\alpha = 0$ deg the reattachment of the flow is already completed. At $x/l = 2.5$ the separation has totally vanished in all flow problems considered. Using the c_f distributions, we see that, as in the inviscid case, the increase in $\Delta\alpha$ affects the flow in the proximity of the surface of the aircraft only within the range $0 \le y/l \le 0.35$.

The downstream shift of the separation region at higher $\Delta\alpha$ values that is caused by the x/l-shift of the shock-boundary-layer interaction is clearly illustrated in Fig. 8. The wall streamlines evidently demonstrate that the separation and reattachment location is a function of span, i.e., in the spanwise direction they move upstream and downstream, respectively. This means that, when considered in the streamwise direction, the reverse-flow region is smallest in the symmetry plane. In the spanwise direction the separation region is generally confined by the edge of the trough. This is also true for the vortex pair upstream of the separated flow regime. Further downstream these vortices overflow the edges of the trough caused by the interaction of the bow shock of the space vehicle with the boundary layer of the aircraft. The knowledge of the location of the reverse-flow regions or, in other words, the shock-boundary-layer interactions is of essential interest to determine the maximum heat loads within the trough and, hence, to develop a sufficient thermal protection system for the upper surface of the lower stage. Compared with the unsteady two-dimensional solutions, the separation does not set in before the trough and is much thinner, such that only very mild compression waves are generated that hardly impair the strength of the orbiter's bow shock.

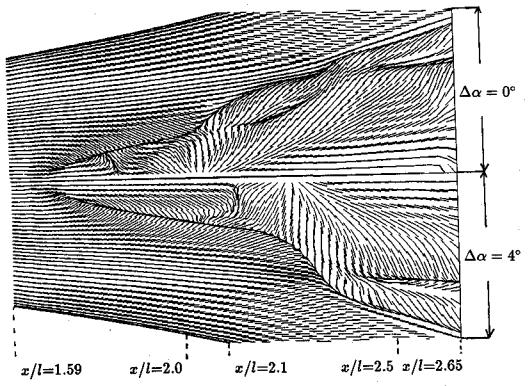

Fig. 8 Wall streamlines on the upper surface of the lower stage at $\Delta\alpha = 0$ deg (top) and $\Delta\alpha = 4$ deg (bottom). The closeup region is defined by the dashed rectangle in Fig. 1.

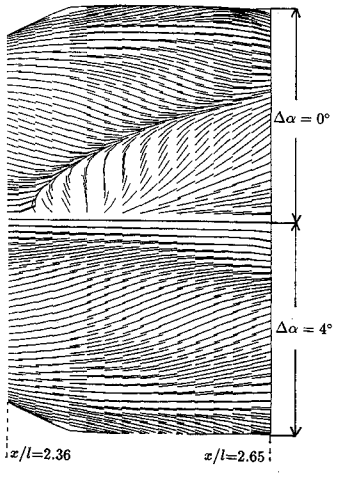

Fig. 9 Wall streamlines on the rear part of the lower surface of the upper stage at $\Delta\alpha = 0$ deg (top) and $\Delta\alpha = 4$ deg (bottom).

As mentioned before, the shock wave deflected from the upper surface of the aircraft affects the flowfield over the space vehicle, i.e., the flow in the proximity of the windward side of the upper stage, only if Δz_r and $\Delta\alpha$ are small. This is clearly illustrated by the wall streamlines on the rear part of the space vehicle's lower surface in Fig. 9. At $\Delta\alpha = 0$ deg the reverse-flow region in the streamwise direction and the spanwise vortices, which occur because of shock-boundary-layer interaction, are encompassed by the C-like-shape separation line. When $\Delta\alpha$ is slightly increased, the separation bubble vanishes and only the vortex pair is retained,[11] and at $\Delta\alpha = 4$ deg the wall streamlines indicate that hardly any interference of the reflected shock wave and boundary layer on the space vehicle's windward surface occurs. In conclusion, this result at a gap width $\Delta z_r = 2.24$ m definitely shows that the larger the incidence angle, the less the impact of the lower stage on the aerodynamic characteristics of the upper stage during the separation maneuver.

Comparison of Numerical and Experimental Results

In the following discussion, we present a comparison of the numerical findings with the experimental data from Esch.[3] Furthermore, we briefly discuss the influence of grid refinement on our numerical results and, finally, we compare perfect and equilibrium real-gas solutions to show the validity of neglecting real-gas effects in the flows considered.

A qualitative experimental-numerical comparison of the flow over the two-stage system at $\Delta\alpha = 0$ and 2 deg can be made by the schlieren photographs in Fig. 10 and the density contours of the inviscid and viscous flowfields in Figs. 2 and 5. Note that in the photographs the shock-boundary-layer

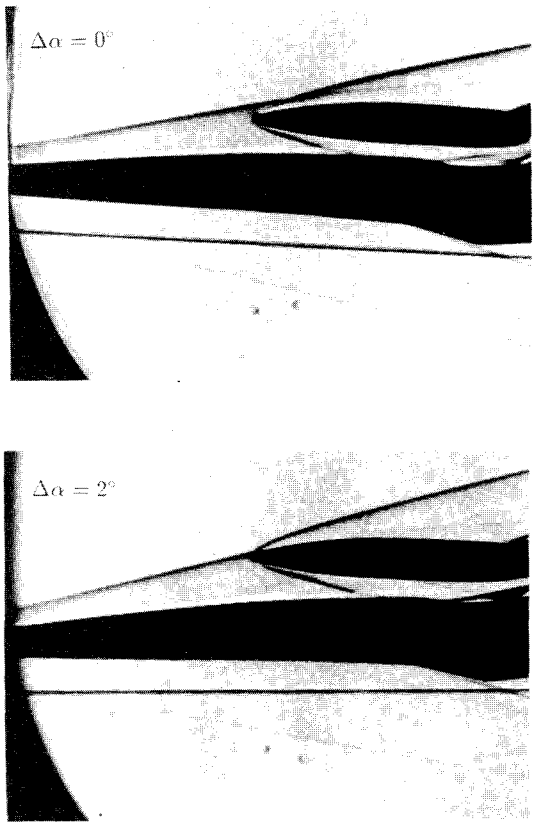

Fig. 10 Schlieren photographs in the symmetry plane at $\Delta\alpha = 0$ deg (left) and $\Delta\alpha = 2$ deg (right).

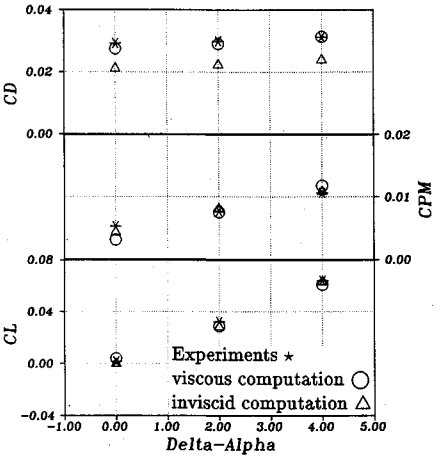

Fig. 11 Aerodynamic coefficients of the upper stage as a function of $\Delta\alpha$.

interaction within the trough is covered by the sidewalls, whereas the sidewalls are not shown in the numerical results. The location of the shock-shock interaction in the vicinity of the nose region of the space vehicle and the slight compression below the lower stage are in good agreement. As far as the flow pattern within the gap is concerned, the correspondence between the Navier-Stokes solutions and the experiment seems to be somewhat better due to the slightly smaller shock angle of the reflected shock wave than that in the inviscid solution. Since in this study we are primarily interested in the aerodynamics of the upper stage, we contrast in Fig. 11 only the measured and computed aerodynamic coefficients of the space vehicle. At all relative angles of attack, c_l and c_{pm} of the experiments and the viscous and inviscid computations agree

Table 1 Numerically determined aerodynamic coefficients of the upper stage at $\Delta\alpha = 2$ deg.

Equations	Mesh	Fluid	c_d	c_l	c_{pm}
Euler	coarse	perfect gas	0.02204	0.02790	0.00781
Euler	fine	perfect gas	0.02232	0.02814	0.00805
Euler	fine	real gas	0.02235	0.02838	0.00803
Navier-Stokes	course	perfect gas	0.02800	0.03198	0.00758
Navier-Stokes	fine	perfect gas	0.02903	0.02873	0.00750

quite well. When viscous forces are neglected, c_d is determined to be approximately 25% less than in the experiment. Of course, this is improved when the solutions of the Navier-Stokes equations are considered. Then the discrepancy with the experimental values is generally less than 5% for c_d, and as such, these numerical results are in satisfactory agreement with the measurements. This means that for the aerodynamic coefficients of the upper stage at a gap width $\Delta z_r = 2.24$ m, the lift and even the pitching moment can be sufficiently accurately computed by solving the Euler equations, whereas solutions of the Navier-Stokes equations have to be calculated if the drag is of equal physical importance. Especially with respect to c_{pm}, however, this result might completely change when the gap width is reduced since, as long as we have supersonic flow within the gap, the less the gap width, the more important the viscous forces for the shock pattern. Furthermore, to develop a thermal protection system for the upper surface of the lower stage, the aerothermal loads on the wall have to be known and, thus, the viscous flow must be computed.

In Table 1 we compiled the aerodynamic coefficients of the upper stage of the inviscid and viscous flowfield at $\Delta\alpha = 2$ deg computed on a fine and a coarse mesh. Obviously, the Navier-Stokes solutions are more susceptible to such a drastic mesh modification, but nevertheless the overall agreement of these integrated values is quite good. The maximum difference is obtained for the lift coefficient and amounts to 3.25×10^{-3}. That is, according to the aerodynamic quantities, only a slight grid dependence can be observed.

We now discuss an inviscid perfect-gas and equilibrium real-gas solution at $\Delta\alpha = 2$ deg. If we use the perfect-gas assumption, the stagnation temperature at $M_\infty = 6$ is $T_0 = 1984$ K. This means that, if equilibrium real-gas effects are encountered at all, they occur in the nose region and on the surface of the upper stage.[12] The little difference in the stagnation temperatures computed for a perfect gas flow $T_{0,p} = 1979$ K and an equilibrium real-gas flow $T_{0,r} = 1888$ K, however, indicates that hardly any real-gas behavior can be observed. Furthermore, the density distributions on the surface of the space vehicle of both computations absolutely coincide,[11] as do the aerodynamic coefficients of these calculations (Table 1). Thus, we conclude that, at the flow parameters considered, the real-gas effects on the inviscid flowfield can be neglected.

Concluding Remarks

A detailed numerical investigation of the inviscid and viscous hypersonic flows over a two-stage space transportation system at several angles of attack between the stages has been made. We used a finite-volume method to integrate the Euler and Navier-Stokes equations for perfect-gas and equilibrium real-gas flows. Because of the satisfactory to good agreement that we obtained in a qualitative and quantitative comparison of numerical and experimental results, in which we contrasted schlieren photographs, density contours, and aerodynamic coefficients, we concluded that our scheme is capable of accurately computing the steady, laminar flow over the two-stage spacecraft at a gap width $\Delta z_r = 2.24$ m. To determine the lift and even the pitching moment of the upper stage it sufficed to solve the Euler equations, whereas the Navier-Stokes equations had to be integrated to predict the drag. The minute analysis of the inviscid and viscous flow showed that the larger the relative angle of attack, the less the impact of the space vehicle on the aircraft and vice versa, i.e., the less the influence of the lower stage on the flight conditions of the orbiter. The comparison of an inviscid perfect-gas and equilibrium real gas flow proved that it is appropriate to neglect real-gas effects in the flow problems considered.

References

[1]Decker, J. P., and Gera, J.,"An Exploratory Study of Parallel-Stage Separation of Reusable Launch Vehicles," NASA TN D-4765, Oct. 1968.

[2]Naftel, J. C., Wilhite, A. W., and Cruz, C. I., "Analysis of Separation of a Two-Stage Winged Launch Vehicle," AIAA Paper 86-0195, Jan. 1986.

[3]Esch, H., "Kraftmessungen zur Stufentrennung am MBB-Sängerkonzept bei Ma = 6 im Hyperschallkanal H2K," DLR Rept. IB-39113-90C18, Cologne, Germany, Dec. 1990.

[4]Schröder, W., and Hartmann, G., "Computation of 3D Viscous Hypersonic Flows," *Proceedings of the 4th International Symposium on Computational Fluid Dynamics,* Vol. II, Davis, CA, 1991, pp. 1035–1040.

[5]Schröder, W., and Hartmann, G.,"Robust Computation of 3D Viscous Hypersonic Flow Problems," *Notes on Numerical Fluid Mechanics,* Vol. 35, July 1992, pp. 128-137.

[6]Schröder, W., and Hartmann, G., "Implicit Solutions of Three-Dimensional Viscous Hypersonic Flows," *Computers & Fluids,* Vol. 21, No. 1, 1992, pp. 109–132.

[7]Yee, H. C.,"Upwind and Symmetric Shock Capturing Schemes," NASA TM 89464, May 1987.

[8]Davis, S. F.,"TVD Finite Difference Schemes and Artificial Viscosity," ICASE Rept. No. 84-20, NASA Langley Research Center, Hampton, VA, June 1984.

[9]Roe, P. L.,"Approximate Riemann Solvers, Parameter Vectors and Difference Schemes," *Journal of Computational Physics,* Vol. 43, No. 2, 1981, pp. 357-372.

[10]Liou, M. S., van Leer, B., and Shuen, J. S.,"Splitting of Inviscid Fluxes for Real Gases," *Journal of Computational Physics,* Vol. 87, No. 1, 1990, pp. 1-24.

[11]Schröder, W., "Analysis of Inviscid and Viscous Hypersonic Flows Past a Two-Stage Spacecraft," MBB Tech. Note TN-KT32-92-0017, MBB AG, Munich, Germany, March 1992.

[12]Anderson, J. D., *Hypersonic and High Temperature Gas Dynamics,* McGraw-Hill, New York, 1989.

Ernest V. Zoby
Associate Editor